

# A Non-deterministic Reconstruction Approach for Isotropic Reflectances and Transmittances

By Gladimir V. G. Baranoski\* and Jon G. Rokne



*Physically and biologically based reflectance and transmittance models add realism to image synthesis applications at the expense of a significant increase in rendering time. Current research efforts in this area focus on developing practical solutions to quickly access a BDF (which represents a combination of BRDF and BTDF) while preserving its original characteristics. In this paper an approach to reconstruct relatively complex isotropic BDFs is presented. The spectral curves obtained using the proposed approach are compared with measured spectral curves, and some issues regarding its performance and storage requirements are examined. Copyright © 1999 John Wiley & Sons, Ltd.*

Received July 1999

KEY WORDS: BDF; BRDF; BTDF; non-deterministic reconstruction methods.

## Introduction

The *bidirectional surface-scattering distribution function* (BSSDF or simply BDF<sup>1</sup>) represents a combination of the *bidirectional reflection distribution function* (BRDF) and the *bidirectional transmission distribution function* (BTDF), which are used to describe the reflectance and transmittance characteristics of materials. It can be determined using a measurement device known as a goniophotometer,<sup>2</sup> or through a computer simulation of such a device, which is called a virtual goniophotometer.<sup>3,4</sup> In both cases a large number of measurements are usually required to represent the BDF accurately. Fortunately, we can often exploit some characteristics of materials and BDF models used in rendering applications to reduce the number of measurements, without decreasing the accuracy of the BDF curves provided by these models. For instance, there are materials with anisotropic characteristics for which there is usually not enough information to support the design of a biologically based anisotropic BDF model. An example is

given by plant leaves.<sup>3</sup> For these cases, since we are working, in practice, with an isotropic BDF model, we need to use only one directional input parameter.

The BDF for a given material can be precomputed using an appropriate scattering model. Afterwards, its stored spectral and directional values can be used to reconstruct the BDF during rendering. The main contribution of this paper consists of a non-deterministic\* approach to reconstruct relatively complex isotropic BDFs. Instead of applying mathematical tools such as wavelets,<sup>6</sup> spherical harmonics<sup>4,7</sup> or interpolation<sup>8</sup> as part of a deterministic strategy, we use a stochastic algorithm based on standard Monte Carlo techniques<sup>5</sup> to reconstruct the BDF. Our goal is to preserve the behaviour and accuracy of the original BDF provided by a BDF model while reducing the costs of its in-line application. We compare the spectral curves obtained using a BDF model in-line with the spectral curves obtained using the proposed reconstruction algorithm.

In our investigation we assume that light propagation is described in terms of ray optics, where light is considered to be composed of non-interacting rays, each of them carrying a certain amount of energy.<sup>9</sup> The BDF measurements are performed using a virtual goniophotometer.<sup>3</sup> As

\*Correspondence to: G. V. G. Baranoski, Department of Computer Science, University of Calgary, 2500 University Drive NW, Calgary, Alberta T2N 1N4, Canada. E-mail: gbaranos@cpsc.ucalgary.ca

Contract/grant sponsor: CNPq (Brazil); Contract/grant number: 200876/93-7.

Contract/grant sponsor: NSERC (Canada); Contract/grant number: 69-1266.

\*In this context we use the terms deterministic and non-deterministic according to how the different approaches select the PDF (*probability distribution function*)<sup>5</sup> used to generate the outgoing distribution of rays associated with a given BDF.

pointed out by Lalonde and Fournier,<sup>6</sup> the use of such a virtual device gives us control over the BDF data generation. It also allows us to capture a BDF at different sampling resolutions and to avoid measurement errors.

The remainder of this paper is organized as follows. The next section introduces the reconstruction approach. The third section presents the testing parameters and procedures. The fourth section discusses the results and performance issues. The paper closes with a summary and directions for further improvements.

### The Reconstruction Approach

Although the proposed reconstruction approach works in the same way for any wavelength channel, a single channel is assumed in order to simplify the following presentation.

#### Data Gathering

The radiance detectors in the virtual goniophotometer used in our investigation are represented by the patches of a collector sphere placed around a specimen. The parametrization of this collector sphere can be performed using different parameter spaces. The advantages and drawbacks of parametrizations commonly used in the context of importance sampling<sup>5</sup> are discussed in a paper by Lafortune and Willems.<sup>10</sup> For the sake of simplicity, in the presentation of the proposed approach we consider the application of the classical  $(\theta, \varphi)$  parameter space, where  $\theta$  and  $\varphi$  represent the azimuthal  $([0, 2\pi])$  and polar  $([0, \pi])$  angles respectively. Using this parametrization, the collector sphere is divided into  $n_t$  patches along its longitudinal axis and  $n_p$  patches along its latitudinal axis.

The parameter space of the BDF function is represented by the input directional parameter space  $S_i$  and the output directional parameter space  $S_o$ . The first is given by the angle of incidence  $\alpha$   $([0, \pi])$  of an incoming ray with respect to the normal of the specimen. The second is given by the azimuthal angle  $\theta$  and the polar angle  $\varphi$ , which define the coordinates of the patches in the collector sphere with respect to the virtual goniophotometer coordinate system (Figure 1).

During the data collection we divide  $S_i$  into  $n_a$  regular intervals which correspond to selected angles of incidence. For each interval we shoot  $N$  rays towards a specimen. The origin of each ray is randomly chosen within the interval. After interacting with the specimen, the rays that

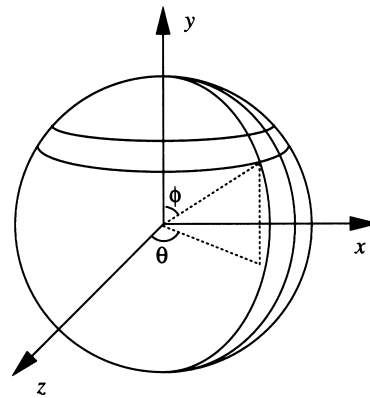


Figure 1. Collector sphere and virtual goniophotometer coordinate system

are not absorbed hit the collector sphere. The total number of rays that were not absorbed is stored in a vector  $V$  of size  $[n_a]$ . The number of hits on each patch is stored in a temporary array  $temp$  of size  $[n_t \times n_p]$ .

Each entry in the array  $temp$  corresponds to a patch and is defined by its row number, which is given by the patch's latitudinal coordinate  $\varphi$ , and its column number, which is given by the patch's longitudinal coordinate  $\theta$ . Afterwards,  $temp$  is linearized and becomes a row in a table  $T$  of size  $[n_a \times n_t n_p]$  (Figure 2(a)), and each patch becomes associated with a number  $j$  that corresponds to its position in a row.

Later on, during the reconstruction process, we need to access the table entry  $T_{ij}$ , where  $i$  is given by the angle of incidence  $\alpha$  and  $j$  is given by the patch's number, to obtain the number of hits received by a certain patch. Before it can be used in the reconstruction process, however, the table  $T$  has to be preprocessed. This preprocessing consists of sorting each row in ascending order and forming the cumulative sum of hits of each element, i.e. each element will contain the sum of the hits of all previous elements

	a)				
	$j=0$	$j=1$	$j=2$	$j=3$	...
$T(\alpha_i, j)$	50	100	20	150	...
	b)				
$T(\alpha_i, j)$	20	70	170	320	...
	c)				
$P(\alpha_i, 0, j)$	$\alpha_2$	$\alpha_0$	$\alpha_1$	$\alpha_3$	...
$P(\alpha_i, 1, j)$	$\beta_2$	$\beta_0$	$\beta_1$	$\beta_3$	...

Figure 2. Example of preprocessing on table T: (a) original row; (b) after sorting; (c) corresponding entries in P

plus its own number of hits (Figure 2(b)). Patches that do not receive any hit are automatically eliminated during this procedure, reducing the storage cost. Since the order of the patches is changed during the sorting, the patches' coordinates  $\theta$  and  $\varphi$  are also stored in a table  $P$  of size  $[2 \times n_a \times n_t n_p]$  (Figure 2(c)). The time required for the preprocessing operation on  $T$  is negligible compared with the data collection and rendering times.

## Reconstruction

Initially, when a ray hits a specimen during the rendering process, we determine the angle of incidence

$$\alpha = \cos^{-1} \left( \frac{\vec{n} \cdot \vec{r}}{|\vec{n}| |\vec{r}|} \right) \quad (1)$$

where  $\vec{n}$  is the specimen normal and  $\vec{r}$  is the direction of the incident ray.

The next step is the generation of a uniformly distributed random number  $\xi$  on the interval  $[0, N]$ . If this random number  $\xi$  is greater than the number of non-absorbed rays stored in  $V(a)$ , we proceed to the next ray, saving valuable time. Otherwise we proceed to the kernel of the algorithm where the reconstruction of the BDF takes place.

In the kernel we perform a search in  $T$  to determine the smallest  $T(a, j) \geq \xi$ . In this way the elements associated with the largest numbers of hits will have the highest probabilities of being selected. Once we determine the row element  $T(a, j)$ , we use  $j$  to obtain the patch's coordinates  $\theta$  and  $\varphi$  stored in  $P(a, 0, j)$  and  $P(a, 1, j)$  respectively. Using these coordinates, the direction of the outgoing ray is given by the angles  $\gamma_m$  and  $\beta_m$ :

$$(\gamma_m, \beta_m) = \left( \theta + \frac{2\pi}{n_t} \zeta_1 \phi + \frac{\pi}{n_p} \zeta_2 \right) \quad (2)$$

where  $\zeta_1$  and  $\zeta_2$  are uniformly distributed random numbers on the interval  $[0, 1]$ .

These angles, in turn, correspond to angular displacements with respect to the  $y$  axis and the  $z$  axis of the virtual goniophotometer coordinate system (Figure 1). Considering that the incident rays are generated during the rendering using a different coordinate system, namely the coordinate system associated with a virtual camera, the generation of the outgoing rays has to be preceded by an appropriate coordinate system transformation.<sup>11</sup>

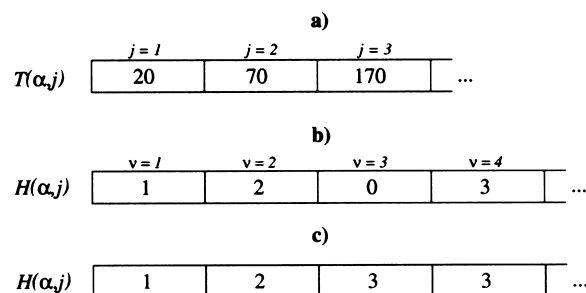


Figure 3. Example of mapping from  $T$  to  $H$ : (a)  $T$ 's row; (b) corresponding row entries in  $H$ ; (c) after postprocessing

## Searching

The searching process mentioned above can be performed using a binary search, which has a worst cost of  $\lfloor \log_2(n_t n_p) \rfloor + 1$  comparisons. However, experiments showed that this strategy was not fast enough for our application. We therefore decided to use a hashing technique instead, in which the column indices of  $T$  are mapped to another table  $H$  of size  $[n_t \times n_r]$  (Figure 3(a)).

For an entry of  $T$  represented by  $T(i, j)$ , the mapping is performed using the following approach:

$$H(i, v) = j \quad (3)$$

where the index  $v$  is given by

$$v = \left\lfloor T(i, j) \frac{n_r}{V(\alpha_i)} \right\rfloor \quad (4)$$

Notice that we may have loss of information related to the mapping from  $T$  to  $H$ . This loss occurs when several column indices  $j$  of  $T$  are mapped to the same entry  $v$  of  $H$ . In this case only the last value mapped is kept in  $H$  and the others are lost. In order to minimize the chances for that to happen, the dimension  $n_r$  has to be greater than  $n_a n_b$ . However, the greater the value assigned for  $n_r$ , the larger are the storage requirements for  $H$ . A reasonable trade-off choice for  $n_r$  is presented in the fourth section.

Before the mapping, the elements of  $H$  are initialized with zeros. After the mapping, some of them may still have zero as their stored value. In order to eliminate the zeros, we postprocess  $H$  by replacing the zero entries in each row by the value of the previous non-zero entry, starting from the row's rightmost element (Figures 3(b) and 3(c)). The time required for the postprocessing operation on  $H$  is also negligible compared with the data collection and rendering times.

During the reconstruction, we use table  $H$  instead of table  $T$  to access the coordinates of a patch associated with  $\xi$ . The patch's position in  $P$  is stored in  $H(a, v)$  and the index  $v$  is computed using the expression

$$v = \left\lfloor \xi \frac{n_r}{V(z)} \right\rfloor \quad (5)$$

### Testing Parameters and Procedures

The data used in our testing experiments correspond to a plant leaf's BDF, which was computed using a BDF model oriented to foliar tissues.<sup>3,12</sup> This choice was motivated by the relative complexity of this BDF, whose behaviour is intermediate to that expected of diffuse and specular reflectors. The collector sphere used by the virtual gonio-photometer was divided into 40 patches along its longitudinal axis ( $n_t=40$ ) and 20 patches along its latitudinal axis ( $n_p=20$ ). The data collection was performed in intervals of  $1^\circ$  for  $S_i(n_a=180)$ . The testing measurements were made using  $10^8$  incident rays per interval and considering the plane given by the incident light and the specimen normal.

The BDF associated with a given radiance detector can be determined in terms of radiant power<sup>13</sup> using the ratio between the radiant power reaching the detector,  $\Phi^r$ , after interacting with the specimen, and the incident radiant power  $\Phi^i$ .<sup>3,14</sup> The corresponding expression used to compute the BDF  $f$  for light incident at wavelength  $\lambda$  is given by

$$f(\lambda, \vec{\omega}_i, \vec{\omega}_r) = \frac{\Phi^r(\lambda)}{\Phi^i(\lambda) \vec{\omega}_r^p} \quad (6)$$

where  $\vec{\omega}_i$  is the solid angle regarding the direction of incidence,  $\vec{\omega}_r$  is the solid angle regarding the direction associated with the detector and  $\vec{\omega}_r^p$  is the projected solid angle regarding the direction associated with the detector.

Consider a total number of  $N$  rays fired towards the specimen for a given wavelength  $\lambda$ . One can assume that each ray carries the same amount of radiant power. Then, as stated by Shirley,<sup>15,16</sup> the radiant power carried by each ray is given by

$$\Phi_{ray}(\lambda) = \frac{\Phi^i(\lambda)}{N} \quad (7)$$

Moreover, the radiant power reaching the detector can be written as

$$\Phi^r(\lambda) = m \Phi_{ray}(\lambda) \quad (8)$$

where  $m$  is the number of rays that hit the detector.

Thus, using equations (7) and (8) in equation (6), the expression to compute the BDF reduces to

$$f(\lambda, \vec{\omega}_i, \vec{\omega}_r) = \frac{m}{N \vec{\omega}_r^p} \quad (9)$$

In turn, the project solid angle  $\vec{\omega}_r^p$  is given by

$$\vec{\omega}_r^p = \frac{A_r \cos \psi_r}{L^2} \quad (10)$$

where  $A_r$  is the area of the detector,  $L$  is the distance from the specimen to the detector and  $\psi_r$  is the angle between the direction associated with the detector and the specimen normal.

The root mean square (RMS) errors,<sup>1</sup> denoted by  $\epsilon$ , of the difference images presented in the next section were computed from normalized pixel values (scaled to [0, 1]) using the expression

$$\epsilon = \sqrt{\frac{1}{p} \sum_{i=1}^{p_x} \sum_{j=1}^{p_y} d^2(x_i, y_j)} \quad (11)$$

where  $p$  is the total number of pixels,  $p_x$  is the number of pixels along the  $x$  axis,  $p_y$  is the number of pixels along the  $y$  axis and  $d(x_i, y_j)$  is the difference regarding the pixels with coordinates  $x_i$  and  $y_j$ .

### Results and Discussion

Figures 4–6 show that the BDF curves obtained through the reconstruction approach agree closely with the measured curves provided by the BDF model. These curves correspond to a selected number of angles of incidence:  $15^\circ$ ,  $30^\circ$  and  $45^\circ$ . The curves for larger angles of incidence and for a larger number of incident rays show similar agreement. Incidentally, the angles were chosen to be less than  $45^\circ$  in order to use the same scale for displaying the curves. The curves for larger angles of incidence would extend much further in the direction of reflection, and they would not fit the editing constraints unless a different scale were used.

The quantitative discrepancies shown in these curves have a small magnitude and suggest that the selected

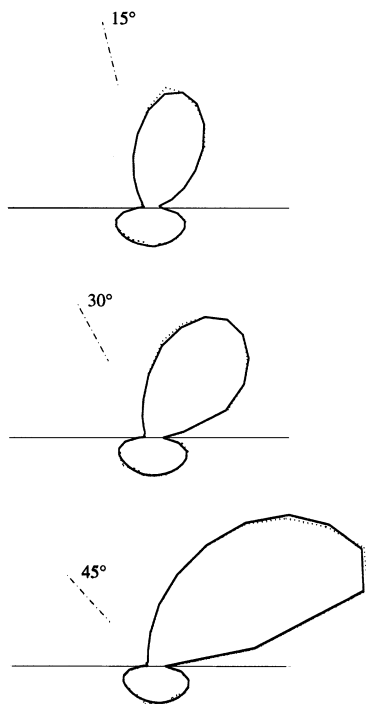


Figure 4. Comparison of BDF curves, at wavelength of 608 nm (red region) and for different angles of incidence, obtained using BDF model (full lines) with curves obtained using the reconstruction approach (dotted lines)

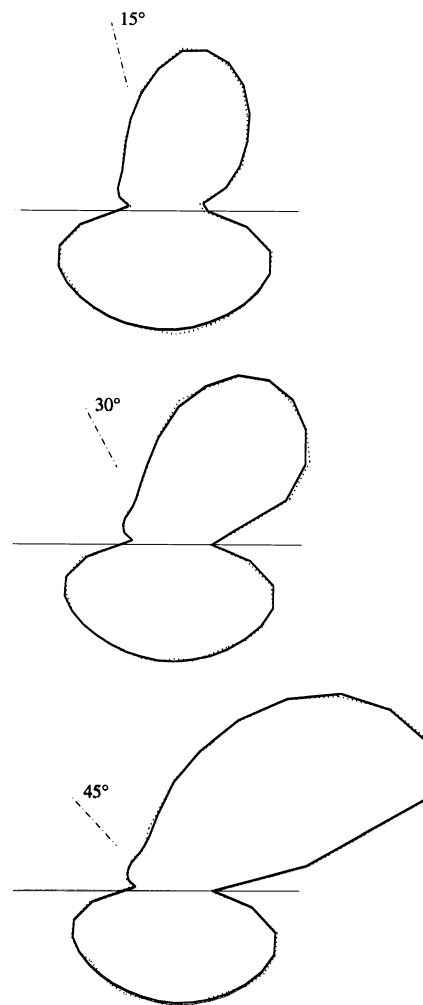


Figure 5. Comparison of BDF curves, at wavelength of 551 nm (green region) and for different angles of incidence, obtained using BDF model (full lines) with curves obtained using reconstruction approach (dotted lines)

sampling resolution determined by the choice of  $n_a$ ,  $n_t$  and  $n_p$  was appropriate for this application. An increase in their values may further improve the accuracy of the results, especially for a BDF that presents discontinuities or high-frequency effects.

Moreover, for rendering purposes, these quantitative discrepancies can be considered negligible, as we can observe in the images presented in Figure 7. These images were generated using a path-tracing rendering algorithm.<sup>17</sup> The corresponding difference image presents an RMS error for the three RGB channels of 0.0123, 0.0131 and 0.0132 respectively.

In order to guarantee that the loss of information (see subsection on Searching) was not a relevant issue in our experiments, we selected a value for  $n_r$  equal to 3560. Then the data structures (vector  $V$  and tables  $P$  and  $H$ ) used by the non-deterministic reconstruction approach occupied 3.1 Mb of memory space for each wavelength channel. This figure represents an acceptable trade-off between storage requirements and accuracy, especially considering the size of the memories available nowadays and their decreasing cost.

The speed-up gain of the rendering process using the proposed approach to reconstruct the leaves' BDF over the process using the BDF model in-line was 51 per cent. The overhead of precomputing the BDFs is minimized by the fact that, for a given material, this operation must be performed only once. After performing this operation, the resulting tables can be used as often as required, not only by the proposed non-deterministic approach but also by deterministic approaches.<sup>4,6,7</sup>

It is important to highlight that the main contribution presented in this paper corresponds to the reconstruction process itself, since the scheme presented to store the BDF representation of a given specimen has been somewhat

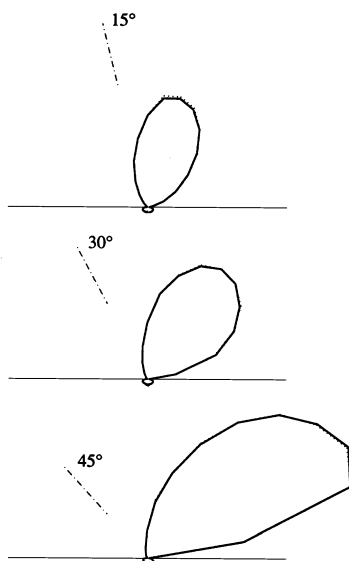


Figure 6. Comparison of BDF curves, at wavelength of 455 nm (blue region) and for different angles of incidence, obtained using BDF model (full lines) with curves obtained using the reconstruction approach (dotted lines)

explored by previous works in the computer graphics literature. For example, Cabral *et al.*<sup>7</sup> used a discrete set of buckets that cover the hemisphere above a specimen to represent its BRDF, and Gondek *et al.*<sup>18</sup> used a geodesic sphere around a specimen to represent its BRDF and BTDF.

Gondek *et al.* also used an adaptive approach to subdivide the facets of the geodesic sphere in order to reduce the storage costs related to the BDF representation. Although this approach seems intuitively to be more efficient than the regular grid of patches over a sphere described in this paper, it requires the implementation of trees and efficient routines for tree traversal. This aspect makes its implementation more complex and may increase the computational overhead substantially.

Recall that during the preprocessing of the storage data structure (see subsection on Data Gathering) the patches that do not receive any hit are eliminated, implicitly discarding elements of the grid that are not relevant for the BDF representation of a given specimen. In other words, the storage scheme presented in this paper, based on a regular grid of patches, also allows an adaptive reduction of the memory costs depending on the BDF representation at hand.

Unfortunately, experimental data regarding performance and storage requirements concerning the application of deterministic approaches are usually not readily avail-

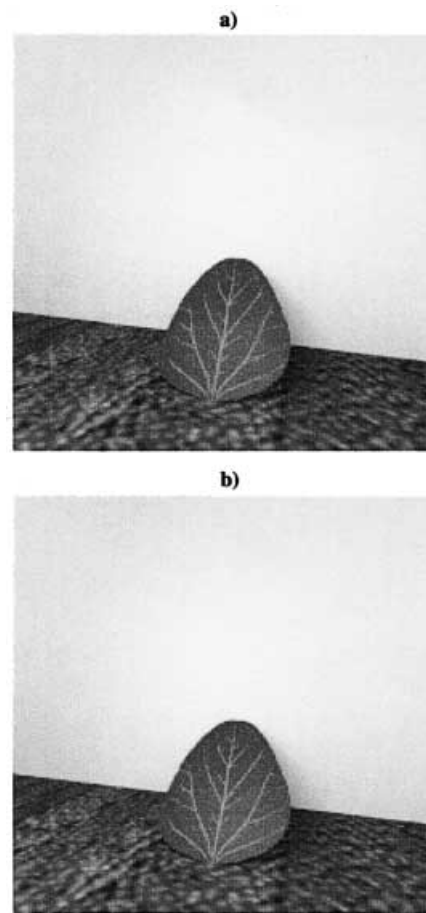


Figure 7. Comparison of images obtained using (a) ABM in-line and (b) non-deterministic reconstruction approach

able in the literature. This aspect makes comparisons of the computational costs involving the application of the proposed non-deterministic reconstruction approach and the deterministic ones more difficult. A comprehensive assessment of their advantages and drawbacks would require a separate investigation, which, in turn, would likely involve the implementation of the different reconstruction techniques and their application to different test cases.

### Summary and Future Work

We have presented a non-deterministic approach for accessing relatively complex isotropic reflectance and transmittance functions. Its simplicity and 'ray nature' enable its straightforward incorporation into Monte Carlo-based rendering systems. The results obtained so far show

that the reconstructed BDF curves present a high degree of accuracy, and the proposed reconstruction approach may provide a noticeable gain in performance while keeping computational costs within reasonable limits.

Finally, since the speed-up gains depend on the complexity of the BDF being reconstructed and on the illuminating and viewing geometries, we intend to extend our evaluation to different materials that present relatively complex BDFs, such as human skin, and different graphics settings in order to establish its full range of applications. This evaluation will also include the analysis of the effects (on storage and computing time) of changing the sampling and model parameters. Future efforts will also involve the extension of the proposed approach to anisotropic materials.

## ACKNOWLEDGMENTS

The authors would like to thank Mark Tigges for his helpful suggestions and the anonymous reviewers for their insights. The work presented in this paper was supported in part by CNPq (Proc. 200876/93-7, Brazil) and by NSERC (Grant 69-1266, Canada).

## References

1. A. Glassner, *Principles of Digital Image Synthesis*, Morgan Kaufmann, San Francisco, CA, 1995.
2. D. Judd and G. Wyszecki, *Color in Business, Science and Industry*, 3rd edn, Wiley, New York, 1975.
3. G. Baranoski and J. Rokne, 'An algorithmic reflectance and transmittance model for plant tissue', *Computer Graphics Forum (EUROGRAPHICS Proceedings)*, **16**(3), 141–150 (1997).
4. S. Westin, J. Arvo and K. Torrance, 'Predicting reflectance from complex surfaces', *Computer Graphics (SIGGRAPH Proceedings)*, **26**(2), 255–264 (1992).
5. J. Hammerley and D. Handscomb, *Monte Carlo Methods*, Wiley, New York, 1964.
6. P. Lalonde and A. Fournier, 'A wavelet representation of reflectance functions', *IEEE Transactions on Visualization and Computer Graphics*, **VCG-3**(4), 329–336 (1997).
7. B. Cabral, N. Max and R. Springmeyer, 'Bidirectional reflection from surface bump maps', *Computer Graphics (SIGGRAPH Proceedings)*, **21**(4), 273–281 (1987).
8. S. Goertler, M. Cohen and P. Slusallek, 'Radiosity and relaxation methods', *IEEE Computer Graphics and Applications*, **14**(6), 48–58 (1994).
9. E. Hecht and A. Zajac, *Optics*, Addison-Wesley, Reading, MA, 1974.
10. E. Lafortune and Y. D. Willems, 'Using the modified phong reflectance model for physically based rendering', *Technical Report*, Department of Computer Sciences, KU Leuven, 1994.
11. J. Foley, A. van Dam, S. Feiner and J. Hughes, *Computer Graphics: Principles and Practice*, 2nd edn, Addison-Wesley, Reading, MA, 1990.
12. G. Baranoski, 'Biologically and physically-based rendering of natural scenes', *PhD Thesis*, Department of Computer Science, University of Calgary, 1998.
13. ANSL, 'Nomenclature and definitions for illuminating engineering', in *ANSI/IES RP-6-1986*, Illuminating Engineering Society of North America, New York, 1986.
14. Y. Govaerts, 'A model of light scattering in three-dimensional plant canopies: a Monte Carlo ray tracing approach', *PhD Thesis*, Département de Physique, Faculté des Sciences, Université Catholique de Louvain-la-Neuve, 1995.
15. P. Shirley, 'Physically based lighting for computer graphics', *PhD Thesis*, Department of Computer Science, University of Illinois, 1990.
16. P. Shirley, 'Time complexity of Monte Carlo radiosity', in F. Post and W. Barth (eds), *Proceedings of the Annual Conference of the European Association for Computer Graphics—EUROGRAPHICS*, North Holland, Amsterdam, 1991, pp. 459–465.
17. J. Kajiya, 'The rendering equation', *Computer Graphics (SIGGRAPH Proceedings)*, **20**(4), 143–150 (1986).
18. J. Gondek, G. Meyer and J. Newman, 'Wavelength dependent reflectance functions', in A. Glassner (ed.), *Proceedings of SIGGRAPH*, ACM Press, 1994, pp. 213–220.